

The crystal structure of anthranilate synthase from *Sulfolobus solfataricus*: Functional implications

(x-ray structure analysis/glutamine amidotransferase/tryptophan biosynthesis)

THORSTEN KNÖCHEL*, ANDREAS IVENS*, GERKO HESTER*, ANA GONZALEZ†, RONALD BAUERLE‡, MATTHIAS WILMANNST, KASPER KIRSCHNER*§, AND JOHAN N. JANSONIUS*§

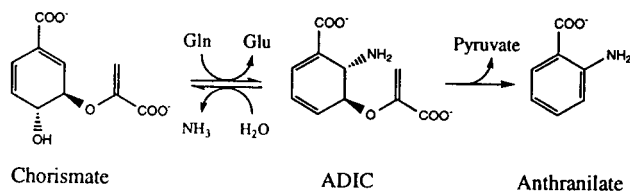
*Biozentrum, University of Basel, Klingelbergstrasse 70, CH-4056 Basel, Switzerland; †European Molecular Biology Laboratory (EMBL) Outstation at the Deutsches Elektronen Synchrotron (DESY), Notkestrasse 85, D-22603 Hamburg, Germany; and ‡Department of Biology, University of Virginia, Charlottesville, VA 22903

Communicated by Charles Yanofsky, Stanford University, Stanford, CA, June 23, 1999 (received for review May 9, 1999)

ABSTRACT Anthranilate synthase catalyzes the synthesis of anthranilate from chorismate and glutamine and is feedback-inhibited by tryptophan. The enzyme of the hyperthermophile *Sulfolobus solfataricus* has been crystallized in the absence of physiological ligands, and its three-dimensional structure has been determined at 2.5-Å resolution with x-ray crystallography. It is a heterotetramer of anthranilate synthase (TrpE) and glutamine amidotransferase (TrpG) subunits, in which two TrpG:TrpE protomers associate mainly via the TrpG subunits. The small TrpG subunit (195 residues) has the known “triad” glutamine amidotransferase fold. The large TrpE subunit (421 residues) has a novel fold. It displays a cleft between two domains, the tips of which contact the TrpG subunit across its active site. Clusters of catalytically essential residues are located inside the cleft, spatially separated from clustered residues involved in feedback inhibition. The structure suggests a model in which chorismate binding triggers a relative movement of the two domain tips of the TrpE subunit, activating the TrpG subunit and creating a channel for passage of ammonia toward the active site of the TrpE subunit. Tryptophan presumably blocks this rearrangement, thus stabilizing the inactive states of both subunits. The structure of the TrpE subunit is a likely prototype for the related enzymes 4-amino 4-deoxychorismate synthase and isochorismate synthase.

Anthranilate synthase (AnthS) from bacteria and yeast is a multifunctional enzyme composed of small TrpG and large TrpE subunits or domains (1). TrpG belongs to the family of “triad” glutamine amidotransferases (2, 3), which hydrolyze glutamine and transfer nascent ammonia through an intramolecular channel to a synthase active site.

The TrpE subunit is a bifunctional enzyme (4). It catalyzes the synthesis of anthranilate in two steps (Scheme 1): the



reversible reaction of chorismate with ammonia to 2-amino 2-deoxyisochorismate (ADIC synthase reaction) followed by the irreversible elimination of pyruvate from ADIC (ADIC lyase reaction). Both reactions require Mg²⁺ ions, and ADIC

is not released into the solvent. The TrpG₂:TrpE₂ complex mediates communication between three distinct ligand-binding sites on the two subunits (1): (i) chorismate binding to the TrpE subunit activates the release of ammonia from glutamine bound to the TrpG subunit; (ii) nascent ammonia is transferred intramolecularly from the TrpG to the TrpE subunit, in preference to ammonia from the bulk solvent (1), and (iii) tryptophan binding to a distinct site on the TrpE subunit (5) inhibits all partial reactions of the TrpG₂:TrpE₂ complex. The strictly ordered addition of chorismate before glutamine (6) and the cooperative binding of both chorismate and tryptophan (7) to the complex suggest that conformational changes mediate the communication between the various ligand-binding sites.

Here, we report the crystal structure of the unliganded AnthS complex from the hyperthermophile *Sulfolobus solfataricus*. The TrpE subunit has a novel fold with distinct binding sites inferred for chorismate and tryptophan. The active sites of the TrpG and TrpE subunits face each other across the intersubunit interface but do not form a channel in the apoenzyme.

MATERIALS AND METHODS

Enzyme Production and Properties. The tandem *trpEG* genes of *S. solfataricus* (8) were cloned from chromosomal DNA into the *Nde*I and *Bam*HI sites of expression vector pET15b (Novagen), which attaches a hexahistidine tag (MGSSHHHHHSSGLVPR ↓ GSHM₁..TrpE) to the N terminus of TrpE subunit and were expressed overnight at 37°C in LB medium in the *Escherichia coli* strain BL21(DE3). AnthS was detectable only in the soluble fraction of cell homogenates (buffer: 0.05 M K₂HPO₄, pH 7.5) and was purified in four sequential steps as follows: (i) heat treatment in the presence of 0.05 M glutamine (9) at 60°C for 25 min; (ii) Ni²⁺-metal chelate chromatography (gradient, 0.02–0.5 M imidazole in buffer); (iii) removal of the hexahistidine tag by trypsin digestion (new N terminus, Gly-3 Ser-2 His-1 Met1. . . ++); and (iv) hydroxylapatite chromatography (gradient, 0.025–0.5 M buffer, containing 0.1 M KCl). The enzyme was >90% pure with a yield of 0.1 mg of protein per liter of culture.

Sedimentation equilibrium measurements ($M_r = 153$ kDa, data not shown) confirmed the calculated M_r [$2 \times (21.9 + 47.7) = 139.3$ kDa], proving that the enzyme is a TrpG₂:TrpE₂ heterotetramer. The enzyme kinetic constants were determined fluorimetrically at 60°C in 0.05 M Tris-HCl (adjusted to pH 7.5 at 60°C), 2 mM MgCl₂, 1 mM DTT, as described by

Abbreviations: AnthS, anthranilate synthase; ADIC, 2-amino 2-deoxyisochorismate.

Data deposition: The atomic coordinates have been deposited in the Protein Data Bank, www.rcsb.org (PDB ID code 1QDL).

§To whom reprint requests should be addressed. E-mail: jansonius@ubaclu.unibas.ch or kirschner@ubaclu.unibas.ch.

The publication costs of this article were defrayed in part by page charge payment. This article must therefore be hereby marked “advertisement” in accordance with 18 U.S.C. §1734 solely to indicate this fact.

PNAS is available online at www.pnas.org.

Tutino *et al.* (ref. 9, their values in parentheses): $K_M^{\text{Chr}} = 0.9$ (3.0) μM , $K_M^{\text{Gln}} = 21$ (19) μM , and $k_{\text{cat}} = 0.14$ (not determined) s^{-1} . Feedback inhibition by tryptophan at 60°C was noncooperative, with $K_i^{\text{Trp}} = 3.3$ (4.0) μM . The enzyme had no detectable glutaminase activity (10) when assayed at 60°C in absence of chorismate and using glutamate dehydrogenase from *Thermotoga maritima* (11) as the coupled enzyme.

Protein Crystallization. Mixing equal volumes of protein solution (15 mg/ml protein in 10 mM K_2HPO_4 buffer at pH 7.5 containing 1 mM EDTA and 0.4 mM DTT) and reservoir solution [1.0–1.5 M NaCl, 2–5% (wt/vol) PEG-6000 buffered with 100 mM K_2HPO_4 buffer at pH 7.5] yielded crystals by vapor diffusion. They belong to space group P6_322 with cell dimensions $a = 162.0$ Å, $c = 212.4$ Å. They contain one TrpG:TrpE protomer per asymmetric unit and have a solvent content of 79% ($V_M = 5.77$ Å³/Da; ref. 12).

Data Collection and Structure Determination. The structure of AnthS was solved by using multiple isomorphous replacement and multiple-wavelength anomalous-dispersion phasing techniques. Mercury derivatives were prepared by soaking crystals in a stabilizing solution (2 M NaCl, 5% PEG-6000, and 20% glycerol in 100 mM K_2HPO_4 buffer at pH 7.5) and 5 mM HgCl_2 for 1–3 days. The lead derivative was prepared by soaking crystals in stabilizing solution containing 15 mM $(\text{CH}_3)_3\text{PbOAc}$ for 12 hours.

Native-I, HgCl_2 -I, and $(\text{CH}_3)_3\text{PbOAc}$ diffraction data were collected on a laboratory rotation anode generator by using $\text{CuK}\alpha$ radiation. Another native data set (Native-II) was collected on the European Molecular Biology Laboratory Outstation at the Deutsches Elektronen Synchrotron (EMBL/DESY) beam line X11 ($\lambda = 0.9095$ Å). A multiple-wavelength anomalous-dispersion data set from a HgCl_2 -soaked crystal (HgCl_2 -II) was collected at four different wavelengths near or at the L_{III} absorption edge of mercury at the EMBL/DESY beam line X31. Wavelengths were selected on the basis of an x-ray fluorescence spectrum of a powder probe of HgCl_2 : λ_1 (1.0055 Å), optimized for f'' with maximal anomalous signal; λ_2 (1.0090 Å), at the inflection point with minimal f' ; λ_3 (1.0247 Å), low-energy remote; λ_4 (0.8500 Å), high-energy remote. All x-ray data were recorded at 100 K on a MAR Research (Hamburg) image plate scanner. Data processing was performed with MOSFLM (13). Integrated intensities were

scaled and merged by using SCALA and AGROVATA (13). Data collection statistics are summarized in Table 1.

Multiple Isomorphous Replacement. The data from the HgCl_2 -I and $(\text{CH}_3)_3\text{PbOAc}$ derivatives were scaled to the Native-I data with SCALEIT (13). Heavy atom positions were determined by difference Patterson and difference Fourier analysis. Final refinement of the heavy atom parameters and phase calculation, including anomalous scattering of the heavy atoms, was performed with SHARP (14). Phases were improved by 120 cycles of solvent flattening with SOLOMON (15). The resulting map was interpretable in most regions of the structure. It was used for model building in combination with a map calculated with phases derived from the isomorphous and anomalous scattering contribution of the mercury derivative (HgCl_2 -II) at four different wavelengths (see below). Multiple-isomorphous replacement-phasing statistics are summarized in Table 1.

Multiple-Wavelength Anomalous Dispersion. SCALA and SCALEIT (13) were used to scale Native-II and HgCl_2 -II data at wavelengths λ_1 , λ_2 , and λ_3 to HgCl_2 -II data at wavelength λ_4 , which was treated as reference data set. Heavy atom parameters as determined by multiple isomorphous replacement (see above) were used as starting model for refinement with SHARP (14). Phases were improved by 120 cycles of solvent flattening with SOLOMON (15). The resulting electron density map was of good quality and was used to trace about 90% of the structure by using O (16). Multiple-wavelength anomalous-dispersion phasing statistics are summarized in Table 1.

Refinement. All data between 30 Å and 2.7 Å of the Native-II data set (reprocessed with DENZO and scaled with SCALEPACK; ref 17; see Table 1) were used to refine the model coordinates with X-PLOR (18). Partial structure factors from a flat bulk-solvent model were applied throughout the refinement (19). After the R factor had converged at 0.234 (free R factor, 5% of data, 0.269; ref. 20), Native-II data were subjected to an overall anisotropic B factor scaling (18). The protein coordinates were subsequently refined against the rescaled Native-II data set. The R factor of the final model is 0.225 (free R factor = 0.253) for all data in the resolution range 30–2.5 Å. The refinement statistics are summarized in Table 2. The structure is well defined in most regions of the polypeptide chains. The electron density is weak for residues 133–140, 247–249, and 301–303, and no interpretable electron density is

Table 1. Data collection and phasing statistics

	MIR phasing			MAD phasing				
	Native-I*	HgCl_2 -I	$(\text{CH}_3)_3\text{PbOAc}$	Native-II†	HgCl_2 -II (λ_1)	HgCl_2 -II (λ_2)	HgCl_2 -II (λ_3)	HgCl_2 -II* (λ_4)
Data collection								
Wavelength, Å	1.5418	1.5418	1.5418	0.9095	1.0055	1.0090	1.0247	0.8500
Resolution, Å	30.0–3.2	30.0–3.2	30.0–3.3	30.0–2.5	30.0–3.1	30.0–3.1	30.0–3.1	30.0–3.0
Unique reflections	27,796	27,407	25,474	56,535 (57,136)	30,551	30,558	30,596	33,525
Redundancy	4.0	3.9	4.7	5.7 (5.3)	3.9	4.1	4.1	4.1
Completeness, %	99.7	97.9	99.8	98.5 (99.8)	99.8	99.8	99.9	99.5
$R_{\text{sym}}^{\ddagger}$	0.089	0.097	0.118	0.063 (0.054)	0.080	0.073	0.072	0.069
Phasing statistics								
R_{iso}^{\S}		0.155	0.111	0.154	0.060	0.056	0.053	
$R_{\text{Cullis}}^{\parallel}$		0.640	0.663	0.672	0.753	0.645	0.689	
Phasing power		2.10/0.83	1.87/0.57	2.10/–	0.21/1.28	1.25/1.11	0.78/0.84	–/1.35

MR, multiple isomorphous replacement; MAD, multiple-wavelength anomalous dispersion.

*Reference data set for scaling and phase determination.

†For refinement, Native II data were reprocessed with DENZO and scaled with SCALEPACK (17). Statistics are given in parentheses.

$\ddagger R_{\text{sym}} = \sum_{hkl} \sum_i |I_i - \langle I \rangle| / \sum_{hkl} \sum_i I_i$.

$\S R_{\text{iso}} = \sum_{hkl} \left(|F_{PH}| - |F_P| \right) / \sum_{hkl} |F_P|$. For data in the resolution range 10.0–3.5 Å. F_P refers to the structure factors of the respective reference data set.

$\parallel R_{\text{Cullis}} = \langle \text{phase-integrated lack of closure} \rangle / \langle |F_{PH} - F_P| \rangle$. For centric reflections, only. F_P refers to the structure factors of the respective reference data set.

$\parallel\parallel$ Phasing power = $\langle \{ |F_H(\text{calc})| / \text{phase-integrated lack of closure} \} \rangle$. For acentric reflections, only. Pairs of values are given for isomorphous and anomalous phasing power, respectively.

Table 2. Refinement statistics

Resolution range, Å	30.0–2.5
Protein atoms, no.	4,870
Water molecules, no.	130
rms deviation bond lengths, Å	0.009
rms deviation bond angles, °	1.446
R factor*	0.225
Free R factor (5% of data)	0.253

$$*R = \frac{\sum_{hkl} ||F_{obs}| - |F_{calc}||}{\sum_{hkl} |F_{obs}|}$$

observed for residues -3, -2 and 33–39 of the TrpE subunit. The latter were not included in the model, and His-1 was

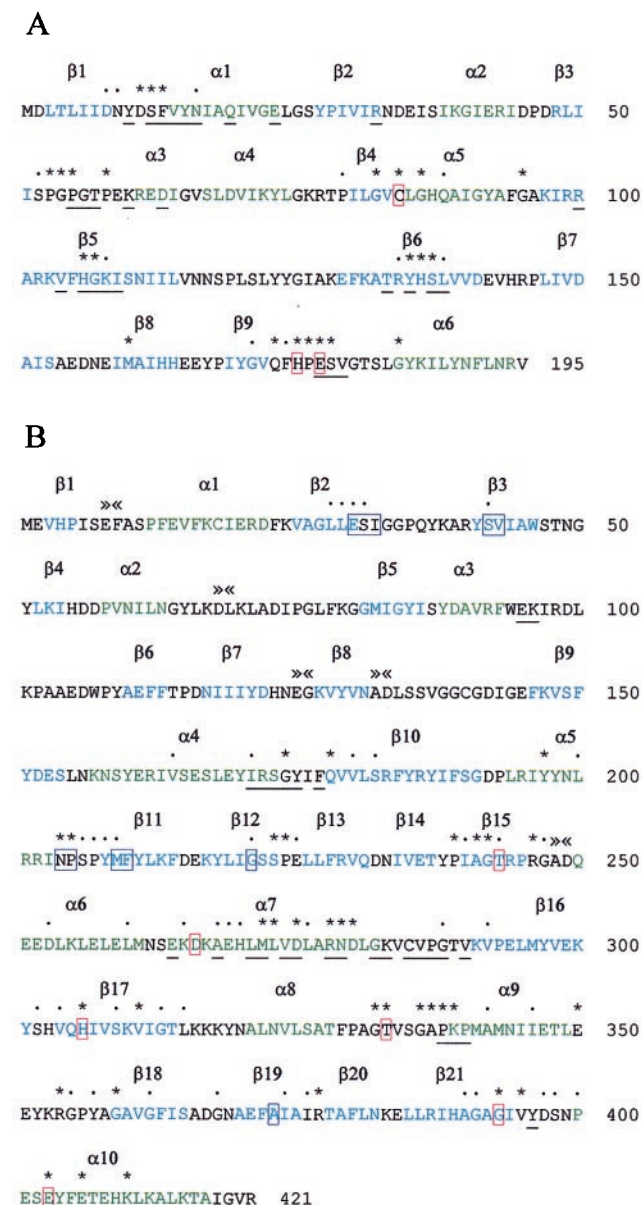


FIG. 1. Amino acid sequence of anthranilate synthase of *S. solfatarius*, with secondary structural elements (defined by DSSP; ref. 22) indicated in blue (β -strands) and green (α -helices). The numbers of these elements appear above the sequences. *, invariant residues; ●, at least 85% conserved residues. (A) TrpG subunit. Red boxes mark the residues Cys-84, His-175, and Glu-177 of the catalytic triad. Residues in contact with the TrpE subunit are underlined. (B) TrpE subunit. Residues corresponding to catalytically important or feedback-sensitive residues in anthranilate synthase of *S. typhimurium* are enclosed in red and blue boxes, respectively. >><<, Sites of deletions compared with TrpE of *S. typhimurium*. Residues in contact with the TrpG subunit are underlined.

modeled as alanine. All residues except Asp-215 and Lys-383 of the TrpE subunit and Cys-84 of the TrpG subunit are in the allowed regions of the Ramachandran diagram (21). The backbone conformations of the residues with disallowed (ϕ, ψ) angles are unambiguously defined by the electron-density map.

RESULTS AND DISCUSSION

Structure and Active Site of the TrpG Subunit. The TrpG subunit has 195 residues (Fig. 1A) and a compact, spherical shape (Fig. 3). The core of the α/β structure of the TrpG subunit is an open, seven-stranded, mixed β -sheet (Fig. 3A and C). The fold is similar to both the N-terminal domain of GMP synthetase (25% sequence identity; ref. 3) and the C-terminal domain of the small subunit of carbamoyl phosphate synthase (23% sequence identity; ref. 24). Structural superposition revealed rms deviations of structurally equivalent C α atoms of 1.31 Å and 1.52 Å, respectively. The residues of the catalytic triad Cys-84, His-175, and Glu-177 are at identical positions, with Cys-84 adopting a similarly unfavorable backbone conformation ($\phi = 60^\circ, \psi = -110^\circ$) as in the two precedents above, ready for catalysis of the glutaminase reaction.

Structure of the TrpE Subunit. The TrpE subunit of AnthS (421 residues; Fig. 1B) has a complicated α/β folding pattern of novel topology (Figs. 2 and 3) with two domains and a cleft. Domain I is composed of residues 1–49, 116–224, and 376–421 and consists of an 11-stranded, antiparallel β -sheet and four helices. Two long inserts, namely subdomain IIA (residues 50–115) between strands β 3 and β 7 and subdomain IIB (residues 225–375) between strands β 12 and β 20, together form domain II. It consists of a nine-stranded antiparallel β -sheet and six helices. All crossover connections of both

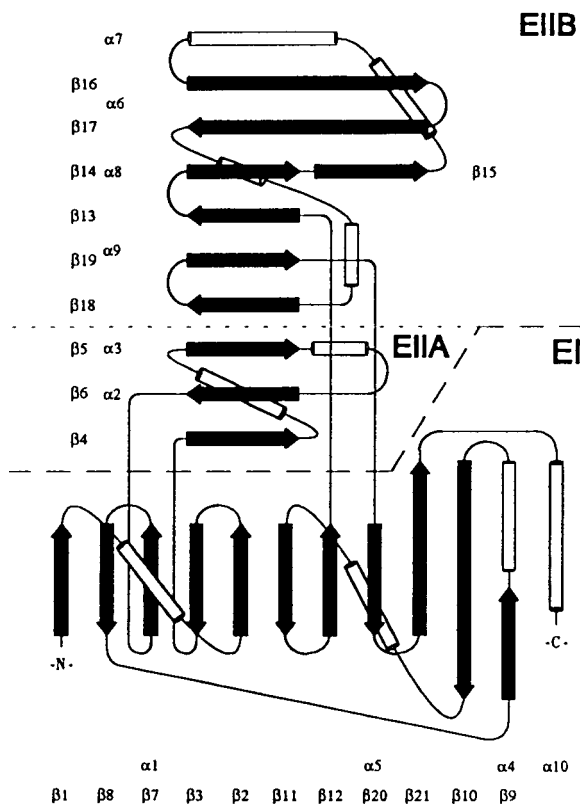


FIG. 2. Topology diagram of the TrpE subunit of anthranilate synthase. The layout corresponds roughly to the view direction in Fig. 3A. β -Strands are depicted as black arrows and α -helices as cylinders. Domain I (green in Fig. 3A) is labeled EI; domain II (yellow in Fig. 3A) is subdivided into the subdomains EIIA and EIIB as described in the text.

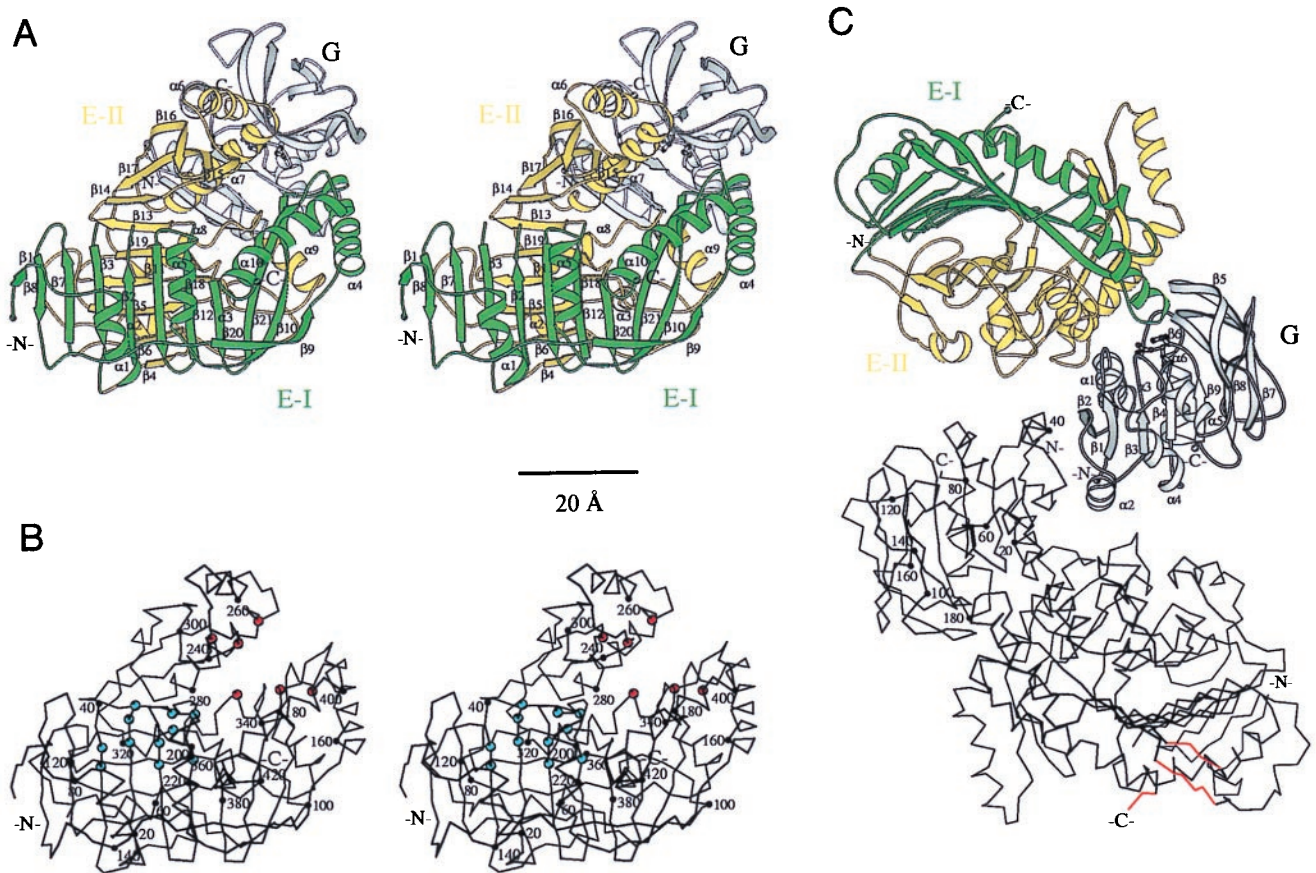


FIG. 3. Three-dimensional structure of anthranilate synthase of *S. solfataricus*. Residues 33–39 (loop $\beta 2\beta 3$) of the TrpE subunit are missing in the model. (A) Ribbon representation of the TrpG:TrpE protomer of anthranilate synthase. Domains I and II of the TrpE subunit are colored green and yellow, respectively. The secondary structural elements of TrpE are numbered. In the TrpG subunit (gray), the catalytic residues Cys-84, His-175, and Glu-177 are depicted in ball-and-stick. (B) C α trace of the TrpE subunit. Every 20th residue (●) is numbered. Residues involved in catalysis and feedback inhibition by tryptophan are labeled by red and blue spheres, respectively. (C) The TrpG₂:TrpE₂ heterotetramer viewed along the crystallographic (and molecular) twofold axis. The top TrpG:TrpE protomer is depicted as ribbon diagram. The secondary structural elements of the TrpG subunit (gray) are numbered, and the catalytic residues Cys-84, His-175, and Glu-177 are depicted in ball-and-stick. The bottom protomer is given as a C α trace, in which every 20th residue (●) of the TrpG subunit is numbered. Regions of the TrpE subunit involved in a crystal lattice contact through an additional crystallographic twofold axis are marked in red. Drawings produced with MOLSCRIPT (23).

domains are right-handed and helical. The β -sheets of both domains have a left-handed twist of $\approx 90^\circ$ (Fig. 3). The strands $\beta 3$, $\beta 2$, $\beta 11$, and $\beta 12$ of domain I together with strands $\beta 6$, $\beta 5$, $\beta 18$, and $\beta 19$ of domain II form an orthogonal β -sandwich with an hydrophobic interface.

The amino acid sequence of the TrpE subunit (8) is 99 residues shorter than that of *Salmonella typhimurium* (1). From the alignment of the two sequences there are five major deletions inferred in the *S. solfataricus* sequence. All are located on the surface of the TrpE subunit (Figs. 1B and 3). Four of the five deletions occur within the first 140 residues, and two of the affected regions (residues 133–140 and 247–249) display weak electron density. These findings are consistent with the observation that thermostable proteins often display shorter surface loops than their thermolabile homologs (25).

Catalytic and Regulatory Sites of the TrpE Subunit. Mutation of the *trpE* gene of *S. typhimurium* has identified six conserved residues (see Fig. 1B) that are important for catalysis (4, 10). The C α positions of the corresponding residues in the TrpE subunit of *S. solfataricus* (Thr-243, Asp-266, His-306, Thr-333, Gly-393, and Glu-403) are located on two internal surfaces of the cleft (Fig. 3B). Similar mutational studies of AnthS from both *S. typhimurium* (5) and *Saccharomyces cerevisiae* (26) have established that residues corresponding to Glu-30, Ser-31, Ile-32, Ser-42, Val-43, Asn-204, Pro-205, Met-209, Phe-210, Gly-221, and Ala-373 of *S. solfataricus* TrpE

(Fig. 1B) are involved in feedback inhibition of AnthS by tryptophan. All but Ile-32, Val-43, and Ala-373 are invariant or conserved. All feedback-sensitive residues except Ala-373 are found in domain I of the TrpE subunit and are clustered on one side of the orthogonal β -sandwich (Fig. 3B). The mean distance between the residues involved in catalysis and feedback regulation (20 Å) confirms earlier evidence (7, 10) that tryptophan and chorismate bind to separate sites. However, the complicated fold of the TrpE subunit (Figs. 2 and 3) rules out the proposal of distinct N-terminal regulatory and C-terminal catalytic domains of the TrpE subunit (5, 7).

Structure of the TrpG₂:TrpE₂ Heterotetramer. Both domains of the TrpE subunit contact the TrpG subunit, close to its active site triad (Figs. 3A and 4). The extensive interface buries 2,730 Å² of surface area and includes 17 invariant or conserved contact residues of 27 in both subunits (Fig. 1). The view of the TrpG:TrpE interface, depicted parallel to helix $\alpha 7$ of the TrpE subunit in Fig. 4A, shows that domain II of TrpE uses helix $\alpha 7$, loop $\alpha 3\beta 6$ and the N terminus of helix $\alpha 9$ as docking surfaces, whereas domain I uses the C-terminus of $\alpha 4$, loop $\alpha 4\beta 10$, and loop $\beta 21\alpha 10$. The view of the TrpG:TrpE interface down the axis of helix $\alpha 7$ of the TrpE subunit (Fig. 4B) shows that the cleft between the two domains of the TrpE subunit is open sideways to solvent. The six catalytically important residues as well as some of the feedback-sensitive residues (Fig. 4B shows Asn-204) of the TrpE subunit are exposed. In contrast, the active site of the TrpG subunit is

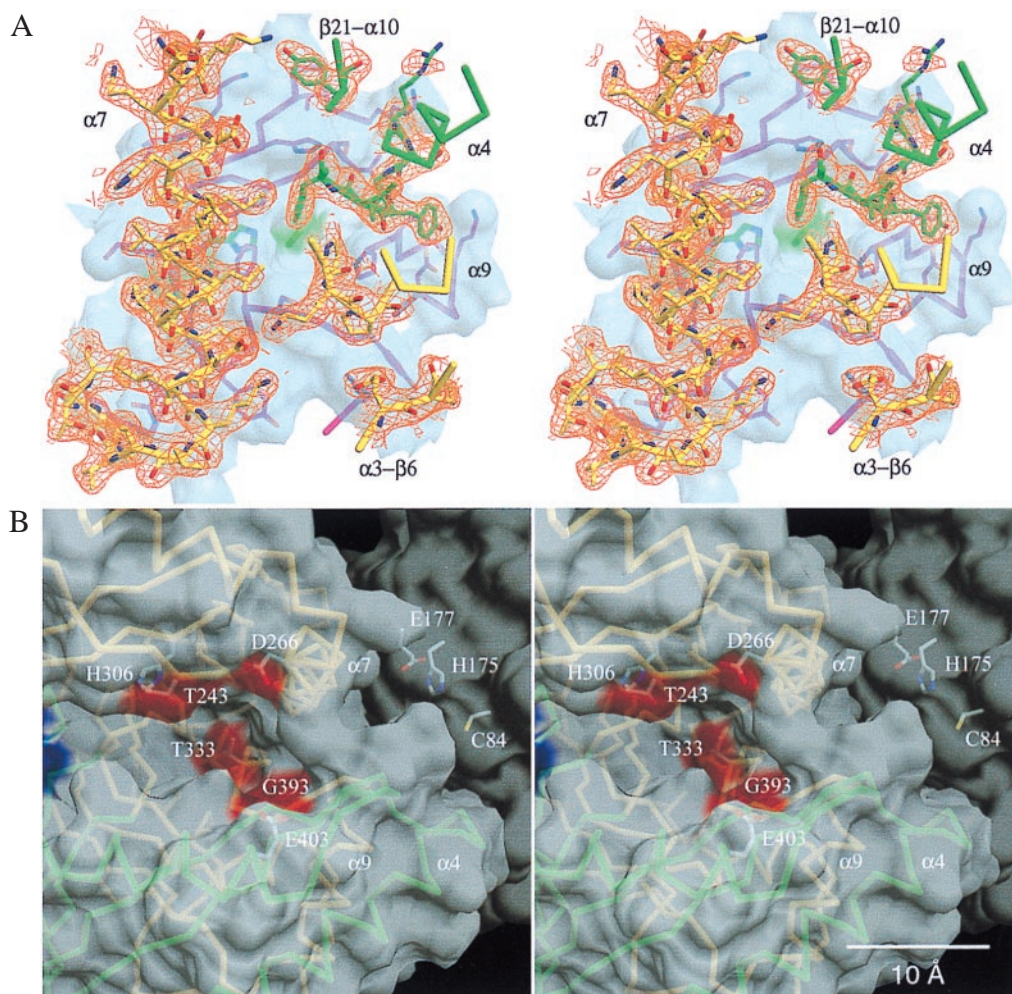


FIG. 4. (A) View of the TrpG:TrpE interface. The $C\alpha$ trace of the TrpE subunit (green for domain I and yellow for domain II) is superimposed on the 2Fo-Fc electron-density map (orange) contoured at 1.0 σ . Secondary structural features of the TrpE subunit are labeled. The TrpG subunit is depicted as a transparent surface in light blue, in which a structural stick model of the contact region of the TrpG subunit is drawn in magenta and atom colors. Residues Cys-84, His-175, and Glu-177 (hidden behind helix $\alpha 7$ of the TrpE subunit) as well as their corresponding surface areas are green. (B) View of the open cleft of the TrpE subunit. To compare the orientation of B to that of A, it is helpful to use the relative positions of helices $\alpha 4$ and $\alpha 7$. Transparent surfaces of the TrpE (light gray) and the TrpG subunit (dark gray) are shown. Surface areas of the TrpE subunit corresponding to residues important for catalysis and feedback regulation are colored red and blue, respectively. The $C\alpha$ trace of the TrpE subunit is shown (green for domain I and yellow for domain II) with helices $\alpha 4$, $\alpha 7$, and $\alpha 9$ labeled. Catalytically important residues of the TrpE subunit and residues Cys-84, His-175, and Glu-177 of the TrpG subunit are depicted in ball-and-stick with atom colors and are labeled. Drawings produced with DINO (A. Philippson, unpublished work; see <http://www.bioz.unibas.ch/~x-ray/dino>).

shielded from solvent. The distance between the groups of catalytic residues in the TrpG and TrpE subunits is about 15 Å.

The two TrpG:TrpE heterodimers are related by a crystallographic twofold rotation axis and are connected via their TrpG subunits (Fig. 3C). The TrpG:TrpG interface buries 1,720 Å² of surface area, suggesting that this interaction corresponds to the tetramerization interface (27). It is predominantly hydrophobic, with seven, albeit nonconserved, side chains contributed by each subunit (Met-1, Leu-3, Tyr-27, Ile-29, Ile-31, Ile-36, and Ile-44). Moreover, the side chains of Glu-35 and Arg-43' (a prime denotes residues of the symmetry-related subunit) are salt-bridged, and the peptide units of Glu-35 and Ser-37' are hydrogen-bonded. An additional lattice contact related to a crystallographic twofold rotation axis is observed between TrpE subunits. It involves residues from $\beta 9$, $\beta 10$, and the C terminus of $\alpha 10$ (compare Fig. 3A and C). Because this crystal contact is more polar than the TrpG:TrpG interface, involves two water molecules, and buries only 1,010 Å² of surface area, it is a less likely tetramerization interface.

The observed noncooperative binding of either chorismate or tryptophan in the *S. solfataricus* AnthS (9) is consistent with the lack of contact between the TrpE subunits in the het-

erotetramer (Fig. 3C). Anthranilate synthases that have additional sequence inserts or additional functional domains and display cooperative ligand binding (e.g., AnthS from *S. typhimurium*; refs. 1 and 4) may have significantly different quaternary structures.

Functional Implications. Catalysis. Combining the information from the crystal structure of AnthS from *S. solfataricus* with reported kinetic and mutational properties of the enzymes from bacteria and yeast leads to new, albeit indirect, insights into the allosteric interactions between the distinct catalytic and regulatory sites of this trifunctional enzyme complex. Of the six catalytic residues identified by mutagenic analysis, three (Thr-243, Asp-266, and His-306) are clustered in subdomain IIB that constitutes the ceiling of the active site cleft (compare Figs. 3B and 4B), whereas the remaining three (Thr-333, Gly-393, and Glu-403) are clustered on the floor of the cleft. The $C\alpha$ atoms of the two groups of residues are separated by 12–18 Å. If these residues were required to be in close proximity for chorismate binding, the cleft would have to narrow, possibly by movement of subdomain IIB (see Fig. 3B). In one scenario, bound chorismate would be tightly sand-

wicked between the identified residues. After conversion of chorismate to ADIC (Scheme 1), the product would remain bound to the original chorismate site, ready for the subsequent ADIC lyase reaction. However, chorismate is a mixed competitive inhibitor of ADIC lyase (4), indicating that chorismate and ADIC can bind simultaneously to the active site, perhaps at close but spatially distinct positions in the cleft of the TrpE subunit. In support of this alternative scenario, mutant enzymes with replacements at any one of the two ceiling residues of the active-site cleft (Asp-266 and His-306) catalyze the synthesis of ADIC from chorismate (Scheme 1) at substantial rates but have negligible ADIC lyase activity (4, 28). However, mutant enzymes with changes at any one of the three floor residues have drastically reduced ADIC synthase and ADIC lyase activities (28). Nevertheless, in both scenarios, anthranilate, a planar molecule that lacks the enolpyruvyl moiety of both chorismate and ADIC, presumably interacts only weakly with the substrate-binding residues.

Allosteric interactions. The closed active site of the TrpG does not allow glutamine to enter (Fig. 4). Moreover, kinetic studies (6) indicate that chorismate must bind first before glutamine can be bound. Because both TrpE domains interact with distinct surface components of the TrpG subunit, close to its active site (Figs. 3A and 4A), conformational changes accompanying chorismate binding could force the TrpG subunit to switch from a nonfunctional to a functional conformation, allowing glutamine to enter and be hydrolyzed at the active site of the TrpG subunit and creating a channel for transferring nascent ammonia to the TrpE subunit. Movement of subdomain IIB may mediate communication between the sites of the TrpE and TrpG subunits. In a similar way, movement of an N-terminal domain of the β -subunit of tryptophan synthase mediates communication between the catalytic sites of the α - and β -subunits (29).

Inhibition of AnthS of both *S. typhimurium* (5–7) and *S. solfataricus* (9) by tryptophan is competitive with respect to chorismate. The distance between the putative binding sites for chorismate and tryptophan (Fig. 3B) suggests that the competition is due to conformational changes that mediate mutually exclusive binding of these ligands. That is, tryptophan binding stabilizes a protein conformation to which chorismate has little or no affinity, and *vice versa*. A simple means for tryptophan to regulate chorismate binding and the activity of the TrpG subunit would be to prevent the putative structural rearrangements that accompany the binding of chorismate. Because diffusion of tryptophan into crystals of AnthS does not crack them, it is likely that the unliganded form of the TrpG₂:TrpE₂ complex, as seen in the crystal structure, has high affinity for tryptophan and low affinity for chorismate.

The Structure of the TrpE Subunit as a Prototype. 4-Amino 4-deoxychorismate synthase (PabB) and isochorismate synthase (EntC) catalyze the conversion of chorismate to closely related analogues of ADIC (Scheme 1; refs. 30 and 31). Moreover, sequence alignments of these proteins with TrpE (32, 33) reveal significant similarities amongst the C-terminal 250 residues (AnthS from *S. solfataricus*/PabB from *S. typhimurium*: 40% identical, 53% similar residues; AnthS/EntC from *S. typhimurium*: 32% identical, 40% similar residues). This most conserved portion of the TrpE sequence is also devoid of insertions and deletions in various TrpE sequences, with one exception (Fig. 1B). Because the catalytic processes and the sequences of the three enzymes are related, the fold of the TrpE subunit is a likely prototype for this group of chorismate-metabolizing enzymes.

We thank H. Szadkowski for excellent technical assistance, I. Thönen for fermentation, A. Lustig for analytical ultracentrifugation, Dr. E. de La Fortelle for advice in using the program SHARP, A. Philippsen for making his program DINO available, and E. Johner for assembling the typescript. We appreciate gifts of *S. solfataricus* cells from Dr. K. O. Stetter, glutamate dehydrogenase of *T. maritima* from Dr. W. M. de Vos, and valuable comments from Dr. J. Smith and an anonymous referee. We thank the staff of the EMBL outstation at DESY for access to their facilities. This work was supported in part by the Swiss National Science Foundation Grants 31-36432.92 to J.N.J. and 31-45855.95 to K.K.

- Zalkin, H. (1993) *Adv. Enzymol. Relat. Areas Mol. Biol.* **66**, 203–309.
- Zalkin, H. & Smith, J. L. (1998) *Adv. Enzymol. Relat. Areas Mol. Biol.* **72**, 87–144.
- Tesmer, J. J. G., Klem, T. J., Deras, M. L., Davisson, V. J. & Smith, J. L. (1996) *Nat. Struct. Biol.* **3**, 74–86.
- Morollo, A. A. & Bauerle, R. (1993) *Proc. Natl. Acad. Sci. USA* **90**, 9983–9987.
- Caligiuri, M. G. & Bauerle, R. (1991) *J. Biol. Chem.* **266**, 8328–8335.
- Zalkin, H. (1973) *Adv. Enzymol. Relat. Areas Mol. Biol.* **38**, 1–39.
- Caligiuri, M. G. & Bauerle, R. (1991) *Science* **252**, 1845–1848.
- Tutino, M. L., Scarano, G., Marino, G., Sannia, G. & Cubellis, M. V. (1993) *J. Bacteriol.* **175**, 299–302.
- Tutino, M. L., Tosco, A., Marino, G. & Sannia, G. (1997) *Biochem. Biophys. Res. Commun.* **230**, 306–310.
- Bauerle, R., Hess, J. & French, S. (1987) *Methods Enzymol.* **142**, 366–386.
- Lebbink, J. H. G., Knapp, S., van der Oost, J., Rice, D., Ladenstein, R. & de Vos, W. M. (1998) *J. Mol. Biol.* **280**, 287–296.
- Matthews, B. W. (1968) *J. Mol. Biol.* **33**, 491–497.
- Collaborative Computational Project Number 4 (1994) *Acta Crystallogr. D* **50**, 760–763.
- de La Fortelle, E. & Bricogne, G. (1997) *Methods Enzymol.* **276**, 472–494.
- Abrahams, J. P. & Leslie, A. G. W. (1996) *Acta Crystallogr. D* **52**, 30–42.
- Jones, T. A., Zou, J.-Y., Cowan, S. W. & Kjeldgaard, M. (1991) *Acta Crystallogr. A* **47**, 110–119.
- Otwinowski, Z. & Minor, W. (1997) *Methods Enzymol.* **276**, 307–326.
- Brünger, A. T. (1992) x-PLOR (Yale Univ. Press, New Haven, CT), Version 3.1.
- Jiang, J.-S. & Brünger, A. T. (1994) *J. Mol. Biol.* **243**, 100–115.
- Brünger, A. T. (1992) *Nature (London)* **355**, 472–475.
- Ramachandran, G. N. & Sasisekharan, V. (1968) *Adv. Protein Chem.* **23**, 283–438.
- Kabsch, W. & Sander, C. (1983) *Biopolymers* **22**, 2577–2637.
- Kraulis, P. J. (1991) *J. Appl. Crystallogr.* **24**, 946–950.
- Thoden, J. B., Miran, S. G., Phillips, J. C., Howard, A. J., Raushel, F. M. & Holden, H. M. (1998) *Biochemistry* **37**, 8825–8831.
- Russell, R. J. M., Ferguson, J. M. C., Hough, D. W., Danson, M. J. & Taylor, G. L. (1997) *Biochemistry* **36**, 9983–9994.
- Graf, R., Mehmman, B. & Braus, G. H. (1993) *J. Bacteriol.* **175**, 1061–1068.
- Janin, J. (1997) *Nat. Struct. Biol.* **4**, 973–974.
- Morollo, A. A. (1995) Ph.D. thesis (University of Virginia, Charlottesville, VA).
- Rhee, S., Parris, K. D., Hyde, C. C., Ahmed, S. A., Miles, E. W. & Davies, D. R. (1997) *Biochemistry* **36**, 7664–7680.
- Walsh, C. T., Liu, J., Rusnak, F. & Sakaïtani, M. (1990) *Chem. Rev.* **90**, 1105–1129.
- Nichols, B. P. (1996) in *Escherichia coli and Salmonella: Cellular and Molecular Biology* (Am. Soc. Microbiol., Washington, DC), 2nd Ed., Vol. 2., pp. 2638–2648.
- Ozenberger, B. A., Brickman, T. J. & McIntosh, M. A. (1989) *J. Bacteriol.* **171**, 775–783.
- Rayl, E. A., Green, J. M. & Nichols, B. P. (1996) *Biochim. Biophys. Acta* **1295**, 81–88.